УДК 539.1

FOCUSING AND IMAGING PROPERTIES OF X-RAY COMPOUND REFRACTIVE LENSES

© 2003 г. V. G. Kohn[1], I. Snigireva[2], A. Snigirev

[1]*Russian Research Centre "Kurchatov Institute", Moscow, Russia*

[2]*European Synchrotron Radiation Facility, Grenoble, France)*

Поступила в редакцию 24.07.2002 г.

Specific features of parabolic compound refractive lenses for X-ray focusing and imaging are discussed theoretically. Relatively large longitudinal size L of refractive lenses requires a verification of the thin lens approximation widely used in the literature. We show that the thick parabolic lens has the focal length $F_l = F + L/6$ measured from the middle of the lens, where F is the focal length in the thin lens approximation. A relatively small aperture of refractive lenses due to absorption of X-rays limits the resolution and, in addition, leads to phase effects visualizing the local phase gradient of the radiation wave field produced by transparent objects. This opens novel technique of imaging for purely phase objects, which is different from the in-line phase contrast imaging techniques. Optical properties of the refractive lens as a Fourier transformer are considered as well.

INTRODUCTION

Since the first demonstration [1] of the X-ray compound refractive lens –CRL) for focusing a synchrotron radiation beam delivered by third generation sources, the X-ray refractive optics is under extensive development. In addition to aluminium [2–9], different low-Z materials: beryllium [2, 5, 7, 9], silicon [10–12], organic compounds [2, 5, 13–18] were experimentally tested. The lens with cylindrical holes drilled in cross geometry allows two-plane focusing [2–4, 14]. The interesting solution is the planar refractive lens with the parabolic profile, which can be either single or compound [10–12]. The lens with circular or parabolic profile and rotational symmetry has a lot of advantages for two-plane focusing and imaging [6, 8, 9, 18]. There are successive attempts to develop the refractive optics by means of various new approaches [19–24]. Significant contributions in the CRL theory are made in [1, 3, 8, 25–27].

Unlike visible light optics, X-ray collecting lens has a concave shape and the material of the lens is always absorbing. This leads to a significant limitation of the CRL effective aperture a_γ even though the physical transverse size a of the lens can be much larger. The CRL has a rather large longitudinal size L so that the thin lens approximation must be verified. Compare to the visible light lens, the ratio a_γ/L for the CRL is very small. This property influences the CRL function as an imaging device. When the ratio a_γ/L is extremely small, the phenomenon like the X-ray beam channeling occurs. However, in most practical cases lenses satisfy the condition $L/F \ll 1$ where F is the CRL focal length in the thin lens approximation. Therefore it is sufficient to consider only the linear corrections in L/F beyond the thin lens approximation.

In this work we present the diffraction theory of the parabolic CRL operating as an imaging device. We explain experimentally observed phase-contrast artifacts in imaging of transparent objects, which becomes visible even in the image plane of the CRL, where the lens formula is fulfilled [28, 29]. These images show up as edge enhanced images, when the boundaries and interfaces of the object generate both bright and dark contrast. These features cannot be explained within the geometrical optics approximation due to diffraction effects.

In the Section 2 we present the detailed theory of the one-dimensional parabolic CRL in terms of the propagators, calculate the CRL propagator in first order L/F approximation, and obtain the total image propagator in the analytical form. We found that the parabolic CRL can be treated as a thin lens placed in the middle of the CRL with the focal length $F_l = F + L/6$. We also discuss properties of the quasi-Fourier image at the back focal plane and the quasi-focused image at the image plane. The computer simulations allow us to confirm the analytical formulas derived. In section 3 we consider the problem of 2D imaging applying the results of the section 2. We show that the CRL 2D propagator is a product of one-dimensional propagators. This property allows one to simplify the problem in many practicable cases.

THE DIFFRACTION THEORY OF ONE-DIMENSIONAL IMAGING WITH PARABOLIC CRL

For the sake of simplicity, we consider one-dimensional case of the in-line setup when the object and the parabolic CRL are homogeneous along the y-axis. Under these conditions, the recorded image or intensity distribution is homogeneous along the y-axis, and we can omit the calculation of the integrals over the y coordinate.

The formulation of the image problem via propagators. We assume the optical axis coincides with the

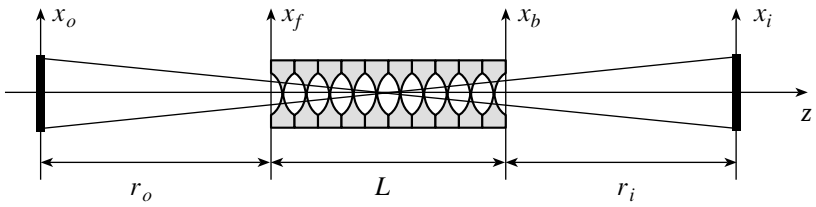

Fig. 1. Geometrical parameters of the experimental setup.

z-axis of the coordinate system (Fig. 1). The *x*-dependence of the complex X-ray wave field including also the incident wave behind the object is described by the complex function $A_o(x_o)$ which hereafter is called the object wave field. We will neglect the longitudinal size of the object compared to the other distances of our setup. The CRL has the parabolic profile of individual components and is located at the distance r_o from the object. The CRL has a length L so that the distance r_o is measured from the object to the front of the CRL.

It is easy to write the *x*-dependence of the complex wave field $A_f(x_f)$ in front of the CRL in terms of the paraxial approximation to the Kirchhoff integral [30]:

$$A_f(x_f) = \int dx_0 P(x_f - x_o, r_o) A_o(x_o). \qquad (1)$$

Here the coordinate x_f is related to the transversal axis in front of the CRL and $P(x, z)$ is the propagator for the transversal *x*-dependence of the field through the free space along the optical *z*-axis:

$$P(x, z) = \frac{1}{(i\lambda z)^{1/2}} \exp\left(i\pi \frac{x^2}{\lambda z}\right), \qquad (2)$$

where λ is a wavelength of the monochromatic wave. Hereafter we imply that the limits of integrals are infinite if the opposite is not specified.

The next step is to calculate the *x*-dependence of the complex wave field behind the CRL. Let us represent the solution through the propagator of the CRL in the form:

$$A_b(x_b) = \int dx_f P_l(x_b, x_f; L) A_f(x_f), \qquad (3)$$

where x_b is the coordinate related for the transversal axis behind the CRL. The complex wave field $A_i(x_i)$ at the image axis, which is placed at the distance ri from the end of the CRL, can be expressed through the Kirchhoff integral once again:

$$A_i(x_i) = \int dx_b P(x_i - x_b, r_i) A_b(x_b). \qquad (4)$$

Substituting eqs. (1) and (3) into eq. (4) and changing the order of integration, we obtain the relation between the object wave field $A_o(x_o)$ and the image wave field $A_i(x_i)$ in terms of the image propagator $G(x_i, x_o)$ as follows:

$$A_i(x_i) = \int dx_o G(x_i, x_o) A_o(x_o), \qquad (5)$$

where

$$G(x_i, x_o) = \int dx_b P(x_i - x_b, r_i) \times \\ \times \int dx_f P_l(x_b, x_f; L) P(x_f - x_o, r_o). \qquad (6)$$

In order to calculate the integral, we need to specify the explicit form of the CRL propagator $P_l(x_b, x_f; L)$.

The *X*-ray compound refractive lens propagator. So far, the thin lens approximation was assumed in the theory of CRL-based imaging, i.e., zero-order approximation in parameter L/F. Violation of this approximation is analyzed within the frame of the geometrical optics and plane wave focusing. In the paraxial approximation the focal length $F = R/2N\delta$, where R is the radius of curvature of the parabola vertex, N is the total number of individual lenses –see Fig. 1, where $N = 10$), and δ is the decrement of the refractive index $n = 1 - \delta + i\beta = 1 - \eta$ [1]. The CRL propagator in this case has a form [3]:

$$P_l(x_b, x_f; L) = \exp[-ik\eta t(x_b)]\delta(x_b - x_f), \\ t(x) = N\left(\frac{x^2}{R} + d\right), \quad L = t\left(\frac{a}{2}\right). \qquad (7)$$

Hereafter $k = 2\pi/\lambda$ is the wave-number, $\delta(x)$ is the Dirac delta-function, $t(x)$ is the variable thickness of the CRL material along the optical axis, d is the minimum spacing between the air parabolic holes, L is the CRL length, and a is the CRL geometrical transverse size. Assuming that a is larger than the effective aperture $a_\gamma = (\lambda F/\gamma)^{1/2}$, where $\gamma = \beta/\delta$, we can neglect the geometrical limits of the CRL.

Our aim is to obtain the CRL propagator in the first-order approximation, i.e. to take into account the corrections linear in L/F. We note that the CRL has a periodic structure of N elements. The period of the structure is L/N. If N is large, the change of the wave field inside the period is relatively small. Therefore we can accept the continual approximation [3] and average the Maxwell's wave equation inside the CRL over the period. Then the total radiation field inside the CRL in the paraxial approximation takes the form $E(x, z) = \exp(ikz)A(x, z)$ and the refractive index $n(x) = 1 - \eta(x)$. Taking into account that $|\eta(-x)| \ll 1$ and applying the paraxial approximation we obtain the parabolic equation for the slowly varying part of the field $A(x, z)$ as follows

$$\frac{dA}{dz} = -ik\eta(x)A + \frac{i}{2k}\frac{d^2A}{dx^2}, \quad \eta(x) = \frac{c}{L}\left(\frac{x^2}{2F} + \delta dN\right), \tag{8}$$
$$c = 1 - i\gamma, \quad \gamma = \frac{\beta}{\delta}.$$

The equation is only valid inside the geometrical aperture of the CRL $|x| < a/2$. Since we assume that the aperture a exceeds the effective aperture a_γ, the region $|x| > a/2$ represents no interest. The equation must be solved inside the interval $0 < z < L$ with the boundary condition $A(x, 0) = A_f(x)$. We are interested in the function $A_b(x) = A(x, L)$.

One can see that the transmission function $\exp(-ik\eta(x)z)$ corresponding to eq. (7) is a solution of the equation (8) if the second term on the right-hand side is negligible. On the other hand, the propagator (2) is the solution of eq. (8) with $\eta(x) = 0$, i.e., in a free space. We try the approximate solution of the eq. (8) in the form $A(x, z) = A_0(x, z)\exp[-ikf(x, z)]$, where:

$$A_0(x, z) = \int dx_f P(x - x_f, z)A_f(x_f),$$
$$\frac{dA_0}{dz} = \frac{i}{2k}\frac{d^2A_0}{dx^2}, \tag{9}$$

and $f(x, z)$ is new unknown function.

The equation for $f(x, z)$ must be solved with the boundary condition $f(x, 0) = 0$. The function $f(x, z)$ is similar to that considered in Ref. [3]. As in the Ref. [3] the approximate solution for $f(x, L) = f_l(x_b, x_o)$ in the first-order approximation in L/F can be derived by iterations and the result is as follows:

$$f(x, L) = \eta L - \frac{L^2}{2}\frac{(x - x_o)}{r_0}\frac{d\eta}{dx} + \frac{L^3}{6}\left(\frac{d\eta}{dx}\right)^2 + \frac{iL^2}{4k}\frac{d^2\eta}{dx^2}. \tag{10}$$

Thus we obtain the propagator of a CRL in the form

$$P_l(x_b, x_f; L) = \exp[-ikf_l(x_b, x_o)]P(x_b - x_f, L). \tag{11}$$

As a result, for the image propagator (6) we have

$$G(x_i, x_o) = \int dx_b P(x_i - x_b, r_i) \times$$
$$\times \exp[-ikf_l(x_b, x_o)]P(x_b - x_o, r_o + L). \tag{12}$$

Here we applied the well known property of the free-space propagator (see discussion in [31]) that the convolution of two propagators is again the propagator for the total distance. We note that the solution (12) does not straightforwardly satisfy the reciprocity principle. More accurate solution that satisfies the reciprocity principle can be obtained but the derivation is more complicated and the difference involves higher orders in small parameter L/F. We will solve this problem below.

Analytical solution for the image propagator. In this section we obtain an analytical expression for integral (12). Taking into account (2), (8) and (10), we can write:

$$G(x_i, x_o) = \frac{C_0}{i\lambda(r_o r_i)^{1/2}}\int dx_b \exp\left(i\frac{k}{2}\varphi(x_i, x_b, x_o)\right), \tag{13}$$

where

$$C_0 = \exp[c(-ik\delta dN + L/4F)],$$
$$\varphi = \varphi_0 + \varphi_1 = U - Vx_b + Wx_b^2. \tag{14}$$

Hereafter we take into account that our accuracy does not exceed first order in L/F. We assume that a correction from distances L in the pre-exponential factor is inessential and the parameter γ is of the same order of smallness as L/F or less.

The parameters $U = U_0 + U_1$, $V = V_0 + V_1$ and $W = W_0 + W_1$ contains the terms of zero and first order in L/F. To satisfy the reciprocity principle, in U_1, V_1 and W_1 we apply the relations between x_o, r_o, x_i, r_i and F resulting from the conditions $V_0 = 0$ and $W_0 = 0$ which correspond to the thin lens formula in zero approximation. At least, this is correct for the imaging problem, because the difference is only due to the terms of higher order in L/F. This way we obtain the expressions for U, V and W in terms of the modified distances:

$$r_{ol} = r_o + L/2, \quad r_{il} = r_i + L/2, \quad F_l = F + L/6, \tag{15}$$

as follows

$$U = \frac{x_o^2}{r_{ol}} + \frac{x_i^2}{r_{il}}, \quad V = 2\left(\frac{x_o}{r_{ol}} + \frac{x_i}{r_{il}}\right),$$
$$W = -\frac{c}{F_l} + \frac{1}{r_{ol}} + \frac{1}{r_{il}}. \tag{16}$$

One can see that all the expressions are symmetrical with respect to the replacement of the object by the image and vice versa. New distances are measured from the middle of the CRL. Correspondingly, the real CRL focal length increases by $L/6$ compared to the thin lens approximation. This result was obtained in Ref. [3] but in the implicit form.

The integral in (13) is calculated applying the table integral, and we arrive at the analytical expression in the form:

$$G(x_i, x_o) = \frac{C_0}{(i\lambda r_g)^{1/2}} \times$$
$$\times \exp\left(i\frac{\pi}{\lambda r_g}[g_i x_i^2 - 2x_i x_o + g_o x_o^2]\right), \tag{17}$$

where

$$r_g = r_{il} + r_{ol} - c\frac{r_{il}r_{ol}}{F_l}, \quad g_i = 1 - c\frac{r_{ol}}{F_l},$$
$$g_o = 1 - c\frac{r_{il}}{F_l}. \tag{18}$$

The analytical solution allows to study the peculiarities of the CRL operation and to understand the difference

between X-ray and light optics. Note that the image propagator $G(x_i, x_o)$ coincides with the free-space one (2): $P(x_i - x_o, r_{il} + r_{ol})$ if $F_l = \infty$ and $C_0 = 1$.

Quasi-Fourier image. As is known in the theory of refractive lenses [30], the complex wave field of the object is converted to the Fourier transform of the wave field at the back focal plane. This is valid approximately for the CRL as well. As follows from the eqs. (5) and (18), the real part of the complex coefficient g_o vanishes when $r_{il} = F_l$ or $r_i = F - L/3$ is fulfilled.

Thus, we conclude once again that the focal length of the thick CRL is redused by $L/3$, if it is taken from the end of the CRL. Correspondingly, the focal length is $L/6$ larger, if it is taken from the middle part of the CRL. Under this condition we have:

$$A_i(x_i) = \frac{C_0 C_1(x_i) C_f(x_i)}{(i\lambda r_f)^{1/2}} \int dx_o \times \times \exp(-iqx_o - \varepsilon x_o^2) A_o(x_o), \tag{19}$$

where $r_f = F_l + i\gamma r_{ol}$,

$$C_1(x_i) = \exp\left(-i\frac{\pi x_i^2 r_{ol}}{\lambda F_l r_f}\right), \quad C_f(x) = \exp\left(i\frac{\pi x^2}{\lambda F_l}\right), \quad q = \frac{2\pi x_i}{\lambda r_f}, \quad \varepsilon = \frac{\pi\gamma}{\lambda r_f}. \tag{20}$$

We note that the parameter r_f is a complex magnitude. Its real part equals F_l whereas the imaginary part is proportional to r_{ol}.

The known result of the visible optics follows from eqs. (19), (20) in the case of infinite aperture and $\gamma = 0$. However, being absorbing the CRL reproduces the Fourier image of the modified object function $A_m(x_o) = A_o(x_o)\exp([-\pi\gamma x_o^2]/[\lambda r_f])$. The more modification is, the larger the parameter γ.

The second CRL feature is that the intensity distribution depends, in the general case, on the distance r_o. In the visible optics of the large aperture the Fourier image is independent of the object position in front of the lens. This property is verified by eqs. (19), (20), if $\gamma = 0$. However, for the CRL $\gamma > 0$, and the Fourier image is conditional because the wave-number parameter q becomes complex. The imaginary part of q can be decreased by placing the object right in front of the CRL when $r_o = 0$.

Let us discuss the quasi-Fourier image in two simple examples. In the first example the object radiates the plane wave $\exp(ikz)$, i.e., $A_o(x_o) = A_o = \text{const}$. The calculation of the integral (19) is straightforward, and we obtain:

$$A_i(x_i) = A_o \frac{C_0 C_f(x_i)}{(i\gamma)^{1/2}} \exp\left(-\frac{\pi x_i^2}{\gamma F_l}\right), \quad \bar{I}_i = \int dx_i |A_i(x_i)|^2 = \left(\frac{\lambda F_l}{2\gamma}\right)^{1/2} |A_o C_0|^2. \tag{21}$$

It is of interest to compare these formulas with the case of a thin transparent lens of the finite aperture a. The result can be obtained from eq. (19) with $C_0 = 1$, $\gamma = 0$, $L = 0$, $A_o(x) = A_o\theta(a/2 - |x|)$. We have:

$$A_{it}(x_i) = A_o\left(\frac{\lambda F}{i}\right)^{1/2} \frac{C_1(x_i) C_f(x_i)}{\pi x_i} \sin\left(\frac{\alpha\pi}{\lambda F} x_i\right), \quad \bar{I}_{it} = \alpha |A_o|^2. \tag{22}$$

According to eq. (21) the intensity $I_i(x_i) = |A_i|^2$ depends on the coordinate xi as the Gaussian with the FWHM $\sigma_\gamma = 0.664(\lambda F\gamma)^{1/2}$ independent of r_o.

Let us compare this value with the diffraction limited resolution $\sigma_a = 0.886\,\lambda F/a$ of the thin transparent lens with the limited aperture a taken from eq. (22). One can determine the effective aperture of the CRL via condition $\sigma_\gamma = \sigma_a$. This leads to the result $a_\gamma^{(1)} = 1.334\,(\lambda F/\gamma)^{1/2}$. Another way is to use the fact that the integral intensity of the focal spot is equal to the aperture for the transparent lens. Then from eq. (21) we obtain $a_\gamma^{(2)} = 0.707\,(\lambda F/\gamma)^{1/2}$. This is approximately twice as less than the preceding determination. Thus there is some difference between the transparent lens of finite aperture and the absorbing parabolic lens.

It is quite enough to use the intermediate value $a_\gamma = (\lambda F/\gamma)^{1/2} \approx 2.51\,(R/\mu N)^{1/2}$ for the CRL aperture. In the second expression we replace F by $R/2N\delta$ and took into account the linear absorption coefficient $\mu = 4\pi\beta/\lambda$. In some works –see, i.e., [16]) the numerical aperture N.A. $= 2(\delta/\mu F)^{1/2}$ is introduced. We see that N.A. $= 1.77\,a_\gamma/F = 1.18\,\lambda/\sigma_\gamma$. We note that the resolution $\sigma_\gamma \longrightarrow 0$ when $R \longrightarrow 0$. This fact was used in [32] for a proposal of micro-ball refractive optics. However, in this case the aperture and the integral intensity are close to zero even for the parabolic shape.

In the second example the object is a very narrow slit, i.e., $A_o(x_o) = A_o\delta(x_o - x_S)$. The calculations is straightforward again and we obtain:

$$A_i(x_i) = A_o \frac{C_0 C_f(x_i)}{(i\lambda r_f)^{1/2}} \times \times \exp\left(-i\pi\frac{x_i}{\lambda r_f}\left[x_i\frac{r_{ol}}{F_l} + 2x_S\right]\right)\exp\left(-\frac{\pi\gamma}{\lambda r_f}x_S^2\right). \tag{23}$$

Now the intensity of x rays $I_i = |A_i|^2$ depends on r_o. If $r_{ol} \approx 0$, $r_f = F_l$ and the intensity does not depend on the coordinate x_i, i.e., it behaves like the Fourier image. However, only the slit positioned inside the aperture

$|x_S| < a_\gamma/2$ can be seen. In the limiting case of a long distance $\gamma r_{ol} \gg F_l$, we can replace r_f by the imaginary value $i\gamma r_{ol}$. Now the intensity distribution differs very much from the Fourier image of the narrow slit and has a maximum value at the point $x_{is} = -x_S F_l / r_{ol}$. The corresponding peak is symmetrical and has the same width as in the case of the plane wave considered above.

Thus we conclude that, in reality, the CRL always transforms the wave field distribution in front of the finite aperture of the CRL. The resolution of the transformation is limited by the diffraction phenomena due to the finite aperture. In the last example the object far removed from the CRL produces approximately the plane wave at the CRL aperture and the image becomes focused instead of showing the Fourier-transform.

Quasi-focused image. Let us consider the CRL image formation when the lens formula $r_{il}^{-1} + r_{ol}^{-1} = F_l^{-1}$ is fulfilled. In this case the real part of r_g vanishes and the CRL propagator (17) reads:

$$G(x_i, x_o) = \frac{C_0}{i}\left(\frac{r_{ol}}{r_{il}}\right)^{1/2} \exp\left(i\frac{\pi}{\lambda}\left[\frac{x_i^2}{r_{il}} + \frac{x_o^2}{r_{ol}}\right]\right)\delta_\sigma(x_o - x_{oi}), \quad (24)$$

where

$$\delta_\sigma(x) = \frac{1}{\sigma(2\pi)^{1/2}}\exp\left(-\frac{x^2}{2\sigma^2}\right),$$
$$\sigma = \frac{\lambda r_{ol}}{a_\gamma (2\pi)^{1/2}}, \quad x_{ol} = -x_i\frac{r_{ol}}{r_{il}}. \quad (25)$$

We note that $\delta_\sigma(x)$ becomes the Dirac delta-function $\delta(x)$ in the limit $\sigma \longrightarrow 0$.

For the transparent lens of infinite aperture we have $\gamma = 0$. Replacing $\delta_\sigma(x)$ by $\delta(x)$, we obtain from eq. (5) the simple relation between the object function $A_o(x_o)$ and the image function $A_i(x_i)$:

$$A_i(x_i) = \frac{C_0}{i}\left(\frac{r_{ol}}{r_{il}}\right)^{1/2} C_i(x_i) A_o(x_{oi}),$$
$$C_i(x) = \exp\left(i\pi\frac{x^2}{\lambda F_l}\frac{r_{ol}}{r_{il}}\right). \quad (26)$$

Thus the image wave field is proportional to the object wave field. However, the shape of the object profile can be increased or decreased. The additional phase factor in the propagator does not influence the intensity in this case. The transparent object remains transparent but the phase profile produced by the object is modified.

The real CRL has a finite imaging resolution σ because $\gamma > 0$. Therefore, even the transparent object can be seen if it produces a drastic perturbation of the phase profile of the incident wave field. The resolution is proportional to the distance r_{ol}. However, in this case we have no possibility to decrease the distance r_{ol}. The lens of the finite aperture makes visible the finite region of the object. We obtain a quasi-image, even if the wave field behind the object is the plane wave, i.e., $A_o(x_o) = 1$. The integral (5) in this case has the analytical expression as $A_i(x_i) = Q(x_i)$, where:

$$Q(x_i) = \frac{C_0}{i}\left(\frac{r_{ol}}{r_{il}p}\right)^{1/2} C_i(x_i)\exp\left(-\frac{\pi}{p}\frac{x_{oi}^2}{a_\gamma^2}\right),$$
$$p = 1 - i\gamma\frac{r_{ol}}{F_l}. \quad (27)$$

When $\gamma r_{ol} \gg F_l$, we arrive at the result (21) again. The point is that $r_{il} \approx F_l$ in this case, according to the lens formula and because of $\gamma \ll 1$. For more practicable case when $\gamma r_{ol} \ll F_l$, we obtain the intensity varying as $I_{ib}(x_i) \approx (r_{ol}/r_{il})\exp(-2\pi x_{oi}^2/a_\gamma^2)$. The size of the visibility region, i.e., FWHM of the intensity distribution, is independent of distances and equal to $a_{ov} = 0.664\, a_\gamma$ in terms of the corresponding coordinate at the object x_{oi}. The physical reason of this phenomenon is due to the image propagator (24), which, in addition to the finite resolution, contains the phase factor $\exp[i\varphi(x_o)]$ with $\varphi = \pi x_o^2/\lambda r_{ol}$ modifying the object wave field.

Let us discuss possible cases of the visibility of transparent objects. We consider first a simple object, which may be called the "phase step". It produces the phase shift $\exp(i\psi)$ in the region $x_S < x_o < \infty$. The general accurate solution reads:

$$A_i(x_i) = \frac{1}{2}Q(x_i)(1 + \exp(i\psi) + S(x_i)[1 - \exp(i\psi)]), \quad (28)$$

where $Q(x_i)$ is determined by (27) and

$$S(x_i) = \left(\frac{2}{i}\right)^{1/2} F_\Phi(Z), \quad Z = \frac{1}{\sigma}\left(\frac{ip}{\pi}\right)^{1/2}\left[x_S - \frac{x_{oi}}{p}\right]. \quad (29)$$

Here

$$F_\Phi(Z) = \int_0^Z dt \exp\left(i\frac{\pi}{2}t^2\right), \quad F_\Phi(-Z) = -F_\Phi(Z) \quad (30)$$

is the complex Fresnel integral. The function $F_\Phi(Z) \approx Z$ for $|Z| < 1$ and $F_\Phi(Z) \approx (i/2)^{1/2}$ for $|Z| > 5$. For typical values of parameters $\gamma r_{ol} \ll F_l$ and $|p - 1| \ll 1$ the center of the image appears at the point $x_i^{(c)} = -x_S(r_{il}/r_{ol})$ corresponding to the modulo minimum value of Z. Assuming that this value is less than unity and replacing $F_\Phi(Z)$ by Z, we obtain:

$$I_i(x_i^{(c)}) \approx I_{ib}(x_i^{(c)})\frac{\cos^2(\psi/2 - \varphi)}{\cos^2(\varphi)}, \quad \mathrm{tg}(\varphi) = -\frac{2x_S}{a_\gamma}, \quad (31)$$

where $I_{ib}(x_i)$ is the background intensity. The formula is valid only for $|\varphi| < 1$. When the point of observation xi moves from the image center $x_i^{(c)}$, the intensity profile restores gradually the background intensity because

$S(x_i) \approx 1$ for x_i far from $x_i^{(c)}$. The region of significant visibility of the "phase step" is $|x_i - x_i^{(c)}| < 5\sigma r_{il}/r_{ol}$.

We note that the intensity within the image region can be lower (dark image) or higher (bright image) than the background. The shape of the image depends on the signs of ψ and x_S. The Eq. (31) allows us to determine the positions of the object with the maximum relative intensity peak or pit. In the region, where $\varphi\psi < \psi^2/4$, the image has the intensity pit. In the region, where the opposite condition is fulfilled, the intensity peak must be observed. The relative peak/pit height increases with increasing the value of $|\varphi - \psi/4|$.

Let us consider now the transparent object which produces an arbitrary smooth phase profile $\psi(x_o)$ having the finite derivatives $\xi_n(x_o) = d^n\psi/dx_o^n$. Since for the given image coordinate x_i the effective region of integration in (5) is $|x_o - x_{oi}| < \sigma$, we can expand the phase in Taylor's series at the point x_{oi} and restrict ourselves only by first three terms,

$$\psi(x_o) \approx \psi(x_{oi}) + \xi_1(x_{oi})(x_o - x_{oi}) + \\ + \frac{1}{2}\xi_2(x_{oi})(x_o - x_{oi})^2. \quad (32)$$

Using the expression (32) for the object wave field $A(x_o) = \exp[i\psi(x_o)]$, we calculate the integral (5) as:

$$A_i(x_i) \approx \frac{C_0}{i}\left(\frac{r_{ol}}{r_{il}p_o}\right)^{1/2} C_i(x_i) \times \\ \times \exp\left(-\frac{\pi}{p_o}\frac{[x_{oi} + X(x_{oi})]^2}{a_\gamma^2}\right), \quad (33)$$

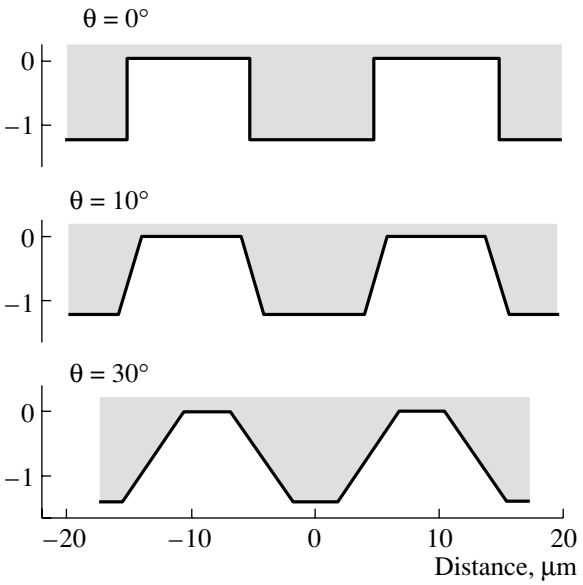

Fig. 2. The central fragments of the phase shift profiles produced by a silicon grid at different rotation angle θ, see the text for details.

where

$$p_o = 1 - i\gamma\frac{r_{ol}}{F_l} - i\xi_2(x_{oi})\sigma^2, \quad X(x_{oi}) = \frac{\lambda r_{ol}}{2\pi}\xi_1(x_{oi}). \quad (34)$$

It is easy to verify that for $\xi_1 = \xi_2 = 0$ we have the result (27).

We note that both the second and the first derivatives of the object phase profile influence the image intensity profile. However, the role of the second derivative is modest, if $|\xi_2(x_{oi})\sigma^2| \ll 1$. On the contrary, the role of the first derivative in the formation of the object image is significant. When $[x_{oi} + X(x_{oi})]^2 > x_{oi}^2$, the intensity decreases compared to the background (dark image). The bright image can be observed in some places where the opposite condition is fulfilled. Of course, when $[x_{oi} + X(x_{oi})]^2 = x_{oi}^2$, the image is determined by the second derivative alone. In the latter case the intensity differs slightly from the background value.

The results of this section demonstrate that the CRL is an excellent device for imaging of transparent objects. However, it shows the image, which is qualitatively different from the image obtained with the in-line setup under the near field condition [34]. The latter technique is based on the eqs. (1), (2) and that the propagator that $P(x, z)$ is approximately $\delta(x)$ for $z \longrightarrow 0$.

Therefore the difference of $P(x, z)$ from $\delta(x)$ is determined by the distance z. In the case of the CRL the distinction of the propagator $G(x_i, x_o)$ from the δ-function is more complicated, namely, it is determined by the finite lens aperture due to absorption. An additional phase factor becomes also essential. The comparison of two techniques for a simple object is made in the next section. Here we note that our results allow to understand the significant difference between phase contrast images of the insect antenna recorded experimentally with and without the CRL (presented in Fig. 4 of [9]).

Computer simulations. To illustrate the analytical results presented above, we choose the simple object as the silicon grid with the following parameters: period $p = 20$ μm, height of rectangular teeth $h = 10$ μm, width of teeth $d = 10$ μm. The grid can be rotated relative the optical axis by the angle θ. The rotation changes the phase profile produced by the object. The calculation is made for the X-ray energy $E = 20$ keV and for the experimental setup with the point source at the distance $r_s = 50000$ m from the object and with the aluminium CRL having the thin lens focal length $F = 1$ m. The very long distance from the source is selected to eliminate some small extra oscillations due to divergence of the beam. However, the divergence of the incident beam does not influence the result which remains practically the same for $r_s = 50$ m. The distances $r_o = r_i = 2$ m. The refractive index parameters are: $\delta = 1.352 \cdot 10^{-6}$, $\beta = 4.21 \cdot 10^{-9}$, $\gamma = 3.12 \cdot 10^{-3}$ for Al and $\delta = 1.21 \cdot 10^{-6}$, $\beta = 4.72 \cdot 10^{-9}$ for Si. Under these conditions $\sigma = 0.35$ μm.

We present the calculation results for three values of the rotation angle θ = 0, 10° and 30°. The fragments of the periodical phase profile produced by the grid are shown in the Fig. 2. In the case θ = 0 the phase profile consists of many positive and negative "phase steps" with $|\psi| = 1.22$. In the case θ = 10° the drastic steps are transformed into small regions of constant phase gradient. In the case θ = 30 the regions of phase gradient become significant. We calculate both the in-line phase contrast images [33] and the images produced by the CRL. In the first case the formulas (1), (2) are used with r_o = 5 cm, where the accurate intensity strongly oscillates. Therefore we convolute the calculated function with the instrumental function which is assumed to be Gaussian with FWHM 0.6 μm.

The results of the computer simulation are shown in Figs. 3–5. The top (a) figures show the phase contrast image. The bottom (b) figures show the CRL image. One can see that the computer simulation confirms all the features of the CRL imaging discussed above analytically. Note that the CRL image shows always the region of the phase gradient in the contrary to the near field phase contrast image. In addition, the CRL image is sensitive to the sign of the phase gradient. As for the "phase step", it can be seen as distinct image with the CRL resolution. These properties mean more single-valued and direct solution of the phase retrieval problem.

The results of the computer simulation for the Fourier transformation of the same object at the different angles of rotation are shown in Fig. 6. In this case $r_i = F$. As it follows from the analytical analysis, we choose $r_o = 0$ to obtain the better image. The top figure shows very many diffraction orders of the periodical grid. All even orders, except zero, are absent due to the structure factor of the grid. Despite the significant difference in maximum all peaks are sharply desplayed. The side peaks are in 10^{-4} times less compared to zero-order peak. The figure at θ = 10 does not contain high-order peaks and the even order peaks become visible. The figure at θ = 30 shows no difference between the peaks of even and odd orders. The high-order peaks are reduced strongly.

As follows from the theory the Fourier transform becomes conditional with increasing the distance r_o. Fig. 7 shows the simulation results of the grid at θ = 0 and r_o = 2 m. The side peaks become damped while the principal orders remain practically unchanged.

THE DIFFRACTION THEORY OF 2–D IMAGING WITH ROUND PARABOLIC XCRL

In this section we show that the wave field distributions along the *x*-axis and *y*-axis propagate independently of each other within the paraxial approximation. First of all, the free-space 2–D propagator is equal to $P^{(2)}(x, y, z) = P^{(1)}(x, z)P^{(1)}(y, z)$ where $P^{(1)}(s, z)$ is determined by eq. (2). Hereafter *s* is any of the coordinate *x* and *y*.

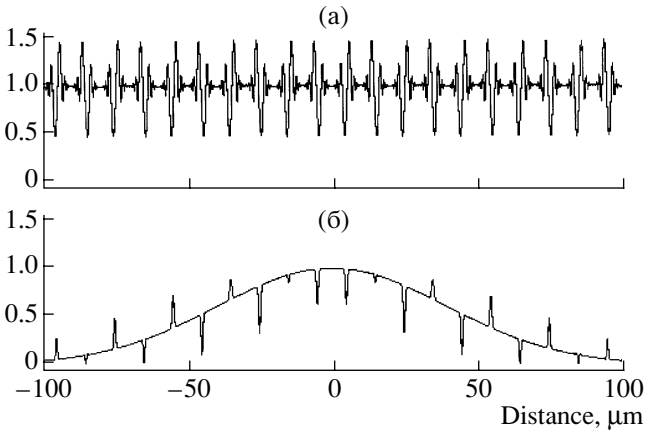

Fig. 3. The normalized intensity distribution (image) for the silicon grid obtained by near field phase contrast technique at 5 cm (top curve) and by the CRL imaging without magnification (bottom curve) at θ = 0.

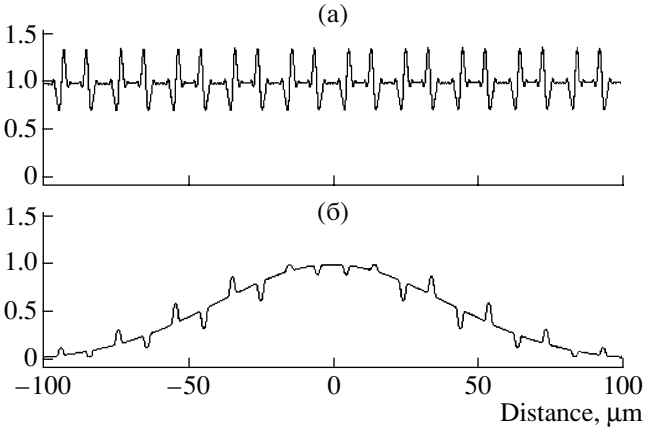

Fig. 4. The normalized intensity distribution (image) for the silicon grid obtained by near field phase contrast technique at 5 cm (top curve) and by the CRL imaging without magnification (bottom curve) at θ = 10.

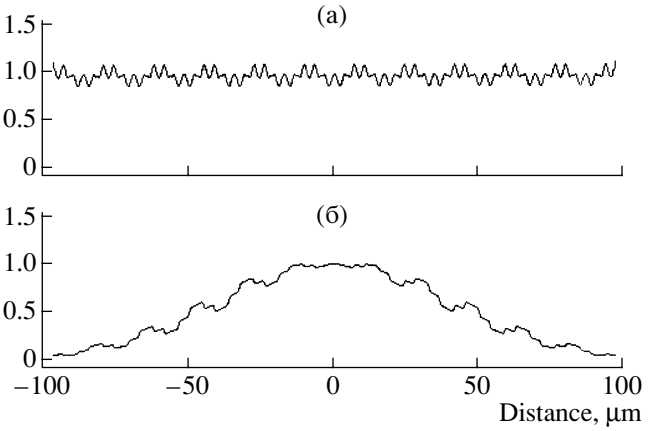

Fig. 5. The normalized intensity distribution (image) for the silicon grid obtained by near field phase contrast technique at 5 cm (top curve) and by the CRL imaging without magnification (bottom curve) at θ = 30.

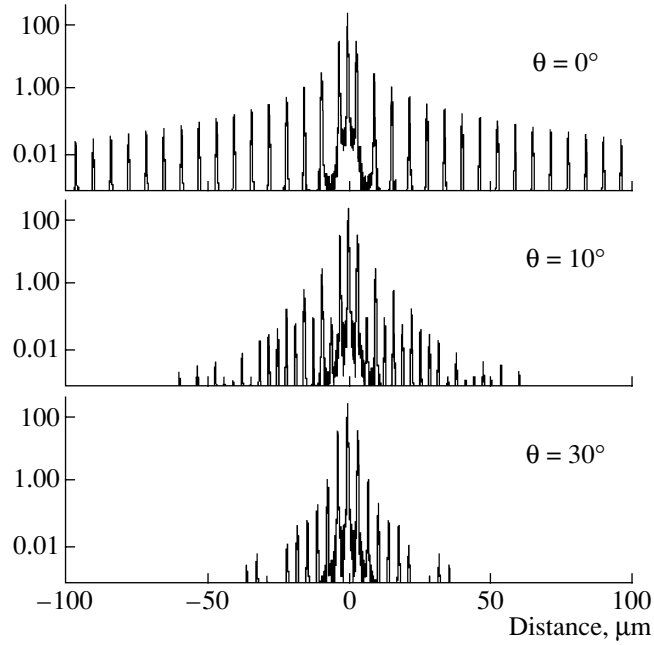

Fig. 6. Decimal logarithm of the normalized distribution of intensity (Fourier transform) recorded at the CRL back focal plane for the silicon grid placed in front of the CRL and for different values of the angle of rotation θ.

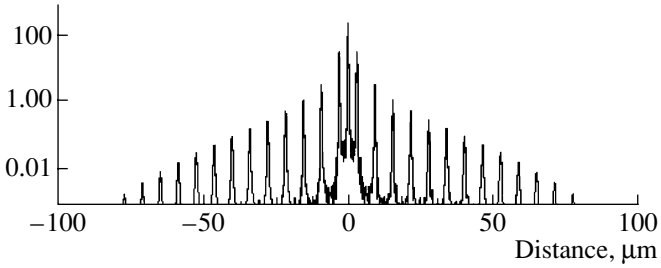

The variable thickness of the round parabolic CRL along the optical axis is equal to:

$$t(x, y) = N\left[\frac{x^2 + y^2}{R} + d\right], \quad (x^2 + y^2) < \frac{D^2}{4}, \qquad L = t\left(\frac{D}{2}, 0\right), \tag{36}$$

where D is a diameter of the CRL aperture. In the thin lens approximation the 2–D propagator can be written as $P_l^{(2)}(x_b, x_f, y_b, y_f) = P_l^{(1)}(x_b, x_f) P_l^{(1)}(y_b, y_f)$ where

$$P_l^{(1)}(s_b, s_f) = \exp\left(-ikc\delta N\frac{d}{2} - ikc\frac{s_b^2}{2F}\right)\delta(s_b - s_f). \tag{37}$$

Thus, the 2D propagator is a product of the 1D propagators. Omitting derivation we note that the CRL 2D propagator has the same property in the linear approximation on L/F as considered above.

This circumstance allows us to calculate the integrals over x and y variables independently. Then, the 2–D image propagator is a product of two 1D propagators $G^{(2)}(x_i, x_o, y_i, y_o) = G^{(1)}(x_i, x_o)G^{(1)}(y_i, y_o)$ where $G^{(1)}(s_i, s_o)$ is determined by eqs. (17) and (18) with replacing d by $d/2$. The general image problem can be formulated as:

$$A_i(x_i, y_i) = \int dx_o dy_o G^{(2)}(x_i, x_o, y_i, y_o) A_o(x_o, y_o). \tag{38}$$

In the general case of an arbitrary object the 2D integral must be calculated and further simplification is impossible.

However, in special cases when the object wave filed is factorisable $A_o(x_o, y_o) = P_o(x_o)Q_o(y_o)$ the image wave field becomes factorisable too $A_i(x_i, y_i) = P_i(x_i)Q_i(y_i)$. The relation between the object wave field and the image wave field can be calculated independently for each axis. It is worthwhile to note that if the lens formula is fulfilled, the propagator is strongly localized. In this case it is sufficient to have an approximate local factorisation of the wave field.4.

CONCLUSIONS

We develop the diffraction theory for the image formation with X-ray parabolic compound refractive lenses in the paraxial approximation. We obtain the analytical expression for the image propagator, which allows us to explain all the features of the CRL operation as an imaging device. We verify the thin lens approximation for the thick CRL of the size L with the linear corrections in L/F. We show that the focal length of the thick CRL measured from the lens center is larger than the thin lens focal length $F = R/2N\delta$ and is equal $F + L/6$.

The relatively small effective aperture of the CRL due to absorption of x rays results in the finite resolution of the image propagator. This explains the experimentally observed property of the CRL to show an image of the transparent object at the distances, which satisfy the lens formula. We discover that such images are associated with the local phase gradient of the X-ray wave field modified by the object. The images are sensitive to the sign of the phase gradient. Thus, the CRL opens new possibility for imaging the transparent objects different from the in-line phase contrast imaging.

We show that the Fourier transformation made by the CRL at the back focal plane becomes conditional due to the finite CRL aperture. The CRL always shows the Fourier transformation of the wave field in front of the lens and modified by the lens aperture. When the object is placed at the long distance from the CRL, the subsequent propagation of the radiation through the free space yields a significant modification of the wave field.

The computer simulations allow us to confirm the analytical formulas. We obtain that the two-dimensional image propagator is a product of two one-dimensional image propagators for x-axis and y-axis. This can simplify calculations of the images for many objects where their structure is described by a product of two functions, each of them represents the separate coordinate axis.

REFERENCES

1. *Snigirev A., Kohn V., Snigireva I., Lengeler B.* // Nature. 1996. V. 384. P. 49.
2. *Snigirev A., Filseth B., Elleaume P. et al.* // SPIE Proc. 1997. V. 3151. P. 164.
3. *Snigirev A., Kohn V., Snigireva I et al.* // Appl. Opt. 1998. V. 37. P. 653.
4. *Elleaume P.* // J. Synchr. Rad. 1998. V. 5. P. 1
5. *Lengeler B., Tummler J., Snigirev A. et al.* // J. Appl. Phys. 1998. V. 84. P. 5855.
6. *Lengeler B., Schroer C.G., Richwin M. et al.* // Appl. Phys. Lett. 1999. V. 74. P. 3924.
7. *Baron A.Q.R., Kohmura Y., Krishnamurty V.V. et al.* // J. Synchr. Rad. 1999. V. 6. P. 953.
8. *Lengeler B., Schroer C., Tummler J. et al.* // J. Synchr. Rad. 1999. V. 6. P. 1153.
9. *Schroer C.G., Lengeler B., Benner B. et al.* // SPIE Proc. 2001. V. 74. P. 274.
10. *Aristov V., Grigoriev M., Kuznetsov S. et al.* // Appl. Phys. Lett. 2000. V. 77. P. 4058.
11. *Aristov V.V., Grigoriev M.V., Kuznetsov S.M. et al.* // Opt. Commun. 2000. V. 177. P. 33.
12. *Aristov V., Grigoriev M., Kuznetsov S. et al.* // SPIE Proc. 2001. V. 4145. P. 285.
13. *Baron A.Q.R., Kohmura Y., Ohishi Y., Ishikawa T.* // Appl. Phys. Lett. 1999. V. 74. P. 1492.
14. *Cremer J.T., Piestrup M.A., Beguiristain H.R. et al.* // Rev. Sci. Instrum. 1999. V. 70. P. 3545.
15. *Piestrup M.A., Cremer J.T., Beguiristain H.R. et al.* // Rev. Sci. Instr. 2000. V. 71, P. 4375.
16. *Beguiristain H.R., Cremer J.T., Piestrup M.A. et al.* // SPIE Proc. 2000. V. 4144. P. 155.
17. *Piestrup M.A., Beguiristain H.R., Gary C.K. et al.* // Nucl. Instr. Meth. B. 2001. V. 173. P. 170.
18. *Ohishi Y., Baron A.Q.R., Ishii M. et al.* // Nucl. Instr. Meth. A. 2001. V.467-468. P. 962.
19. *Dudchik Yu.I., Kolchevskii N.N.* // Nucl. Instr. Meth. A. 1999. V. 421. P. 361.
20. *Kohmura Y., Awaji M., Suzuki Y. et al.* // Rev. Sci. Instr. 1999. V. 70. P. 4161.
21. *Dudchik Yu. I., Kolchevsky N. N. et al.* // Nucl. Instr. Meth. A. 2000. , V. 454. P. 512.
22. *Dudchik Yu.I., Kolchevsky N.N.* // SPIE Proc. 2001. V. 4145. P. 235.
23. *Cederstrom B., Cahn R., Danielsson M. et al.* // Nature. 2000. V. 404. P. 951.
24. *Cederstrom B., Danielsson M., Lundqvist M.* // SPIE Proc. 2001. V. 4145. P. 294.
25. *Protopopov V.V., Valiev K.A.* // Opt. Commun. 1998. V. 151. P. 297.
26. *Protopopov V.V.* // Opt. Commun. 1999. V. 172. P. 113.
27. *Pantell R.H., Feinstein J., Beguiristain H.R. et al.* // Rev. Sci. Instr. 2001. V. 72. P. 48.
28. *Schroer C. G., Benner B., Gunzler T. F. et al.* // SPIE Proc. 2002. V. 4503. to be published.
29. *Weitkamp T., Rau C., Snigirev A.* // SPIE Proc. 2002. V. 4503. to be published.
30. *Born M., Wolf E.* Principles of Optics, 7-th ed. Cambridge, U.K.: Cambridge University Press, 1999. 450 p.
31. *Kohn V. G.* // Phys. Scripta. 1997. V. 56. P. 14.
32. *Girardeau-Montaut J.-P., Girardeau-Montaut C.* // Opt. Commun. 2001. V. 198. P. 1.
33. *Snigirev A., Snigireva I., Kohn V. et al.* // Rev. Sci. Instr. 1995. V. 66. P. 5486.

ФОКУСИРУЮЩИЕ И ИЗОБРАЖАЮЩИЕ СВОЙСТВА РЕНТГЕНОВСКОЙ СОСТАВНОЙ РЕФРАКЦИОННОЙ ЛИНЗЫ

В. Г. Кон, И. Снигирева, А. Снигирев

Теоретически анализируются специфические свойства параболических составных рефракционных линз для фокусировки и изображения с помощью рентгеновских лучей. Из-за относительно большой продольной длины L рефракционных линз необходимо уточнить приближение тонкой линзы, широко используемое в литературе. Мы показали, что толстая параболическая линза имеет фокальную длину $F_l = F + L/6$ при измерении её от середины линзы, где F – фокальная длина в приближении тонкой линзы. Относительно малая апертура рефракционной линзы из-за поглощения рентгеновских лучей ограничивает разрешение и дополнительно приводит к эффекту визуализации локального градиента фазы волнового поля излучения после прохождения прозрачного объекта. Это позволяет развить новый метод визуализации чисто фазовых объектов, отличающийся от фазоконтрастного метода на просвет. Рассмотрены также оптические свойства рефракционной линзы как Фурье-трансформатора.